Effect of Infrared Pulse Excitation on the Bound Charge Transfer State of Photovoltaic Interfaces

Yun Geng[†,‡], *Myeong H. Lee*[†,‖] *and Alessandro Troisi**[,‖]

[†] Department of Chemistry, University of Warwick, Coventry CV4 7AL, U.K.

[‡] Institute of Functional Material Chemistry, Faculty of Chemistry, Northeast Normal University, Changchun 130024, P. R. China

[‖] Department of Chemistry, University of Liverpool, Liverpool L69 7ZD, U.K.

Corresponding Author

*A. Troisi: E-mail: a.troisi@liverpool.ac.uk

ABSTRACT

The nature and dynamics of the bound charge transfer (CT) state in the exciton dissociation process in organic solar cell is of critical importance for the understanding of these devices. It was recently demonstrated that this state can be probed by a new experiment where an infrared (IR) push-pulse is used to dissociate charges from the bound excited state. Here we proposed a simple quantum dynamics model to simulate the excitation of IR pulse on the bound CT state with model parameters extracted from quantum chemical calculations. We show that the pulse dissociates the CT state following two different mechanisms: one, fairly expected, is the *direct* excitation of higher energy CT states leading to charge separation; the other, proposed here for the first time, is a *rebound mechanism* where the negative charge is transferred in the opposite direction to form the neutral Frenkel exciton state from where it dissociates.

TOC GRAPHIC

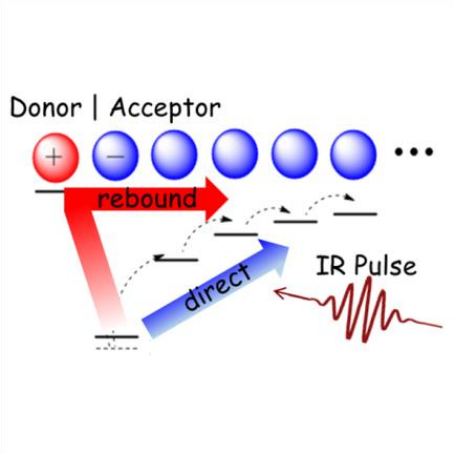

The mechanism of exciton dissociation into free charge carriers at the donor/acceptor interface of an organic photovoltaic device is still under dispute.[1-5] A number of mechanisms have been proposed to describe the process of generating free charges from an excitation residing in the donor material and these include the delocalization of 'hot' charge transfer (CT) state,[6-9] the role of interfacial polarization,[10-13] the contributions of entropy and disorder[7,14-16] with electron dynamics ranging from coherent[2,17-21] to incoherent.[19,22-24] A somewhat disconnected line of investigation involves the study of the bound CT state, i.e. the state where hole and electron in the donor and acceptor materials are close to the interface between the two. The accepted viewpoint seemed to be that the most likely fate of the bound CT state is the charge recombination to the ground state, which is essentially the main dissipation process. However, it was also demonstrated experimentally that the lowest-energy CT state could also generate free carrier with a very high (~90%) quantum yield.[25,26] This prompted a number of studies into the nature and dynamics of the bound CT state which can help elucidating the basic mechanism of charge separation in organic solar cell.[1,12,21,22,27-38]

Recently, Friends and his group introduced the pump-push-photocurrent experiments on some organic solar cell devices, in which the pump pulse leads to bound CT states and the push pulse is used to probe these states and give them a second chance to dissociate.[6,39,40] The bound CT states were found to separate into free carriers with the push of IR pulse being followed by an increase of charge collected at the electrodes. The renewed interests in the importance of the CT states prompted a number of theoretical works[15,31,37] focusing for example on the efficient charge separation of cold CT states,[22] the nonradiative recombination of the lowest CT state,[29] and the coexistence of bound localized CT states with thermally accessible delocalized space-separated states.[41] Building a quantum dynamics model for CT states and considering a CT state with

intermediate range electron-hole separation provide a good model for the competition between charge separation and recombination.[42]

These past theoretical studies, however, did not consider the effect of probing spectroscopically the bound CT states and cannot be used to interpret the pump-probe experiments. In this letter, we carried out a quantum dynamics simulation of the excitation of the bound CT state with an IR pulse by building a simple one-dimensional model Hamiltonian. The influences of different parameters were explored to investigate the role of push-pulse and find the critical factors determining the fate of bound CT state and the charge separation mechanism in this particular experiment.

A one-dimensional phenomenological model was constructed as shown in Figure 1, in which hole is localized at the donor and electron can transfer between the acceptors. Each charge transfer state (CT_n) corresponds to the electron reaching the *n*th accepter, wherein the hole and electron are bound by the Coulombic interaction. Thus, the CT states in this model can be marked by the acceptor sites where the electron is localized.

The total Hamiltonian consists of system Hamiltonian $\hat{H}_S$ and the system-field interaction term (the influence of push pulse) $\hat{H}_{SF}$. The system Hamiltonian can be described as follows:

$$\hat{H}_S = \sum_{i=1}^{N} E_i |i\rangle\langle i| + E_{\mathrm{FE}} |0\rangle\langle 0| + E_{1^*} |1^*\rangle\langle 1^*| + \left(\sum_{i=1}^{N-1} V |i\rangle\langle i+1| + V |0\rangle\langle 1| + V |2\rangle\langle 1^*| + h.c. \right) \quad (1)$$

wherein $|i\rangle$, $|0\rangle$ and $|1^*\rangle$ represent the *i*-th CT state, Frenkel exciton (FE) state, and the excited state of CT_1 state (CT_1*), respectively; $E_{i(\mathrm{FE},1^*)}$ is the electronic site energy of acceptor *i* (FE, CT_1*); *V* is the electronic coupling between adjacent sites, assumed to be the same for all adjacent sites and controlling the bandwidth of the acceptor material; and *N* is the total number of acceptor sites. In equation (1), we added the states that could be excited with an IR push pulse,

i.e., not only CT_2 but also FE state that can be formed optically as a charge transfer excitation and CT_1*, which is obtained by exciting the anion in the bound hole-electron pair leaving a net electronic charge on site 1, (CT_1* turns out to be not important for the remainder of our discussion but it is present in the IR absorption of fullerene acceptors when their charge is –1). Therefore, the electronic couplings include not only the term between the nearest neighboring CT states ($|i\rangle\langle i+1|$) but also the ones between the FE and CT_1 state ($|0\rangle\langle 1|$) and between the CT_2 and CT_1* state ($|2\rangle\langle 1^*|$).

The experimental IR push-pulse was simulated by the interaction of system with an external laser field. It can be expressed in the electronic dipole approximation as

$$\hat{H}_{SF} = -\hat{\mu} E_{ext}(t) \qquad (2)$$

where $E_{ext}(t)$ is the electric field of the pulse, represented in this work as

$$E_{ext}(t) = E_0 \exp\left(-\frac{(t-t_0)^2}{2\sigma_p^2}\right)\cos(\Omega_L t) = E_0 \exp\left(-4\ln 2\frac{(t-t_0)^2}{2\tau_p^2}\right)\cos(\Omega_L t) \qquad (3)$$

where E_0, t_0, σ_p, Ω_L and τ_p are the field intensity, pulse center, pulse width, pulse frequency and the full pulse width at half maximum (FWHM), respectively.

It is assumed that IR pulse reaches the system after it has relaxed to the lowest eigenstate which is therefore the initial states of the simulation,[41,43,44] an assumption justified by the relatively long time delay between pump and push pulse, varying from tens to hundreds of picoseconds. It can be clearly seen from the equations (1) - (3) that many physical parameters are involved in our model Hamiltonian, and their definition and setup are important to the results. The relative energy of FE state to CT_1 state is set as 0.3 eV referred to the results of DFT

calculation on typical P_3HT/PCBM interface, which is detailed in supporting information (SI). The transition dipole moment operator in equation (2) can be written by $\hat{\mu}=\mu'|1\rangle\langle 0|+\mu''|1\rangle\langle 1^*|+\mu'''|2\rangle\langle 1^*|+\sum_{i=1}^{N-1}\mu|i\rangle\langle i+1|+h.c.$, where μ' is the transition dipole moment between the FE and CT_1 state, μ''/μ''' is the transition dipole moment between the CT_1* and CT_1/CT_2 state, and μ is the transition dipole moment between the nearest neighbors. In our calculation we set all transition dipole moments to the same value, i.e., $\mu=\mu'=\mu''=\mu'''$, based on the DFT calculation performed on two molecular models (see SI for details). We set μE_0 = 5 meV, which leads to a few tenth of population transition from the initial state. The pulse center t_0 and the FWHM τ_p were set to 0.1 and 0.15 ps, respectively.[38] The site energy E_i in equation (1) is determined by Coulomb binding energy, $E_i=-\frac{e^2}{4\pi\varepsilon_0\varepsilon i\mathrm{L}}$, where the relative dielectric constant ε and the distance between neighboring acceptors (L) are set to 3.5 and 13 Å, respectively, which are close to the experimental values reported for typical organic photovoltaic devices. We explore the influence of important parameters, such as the pulse frequency Ω_L and the electronic coupling V, where Ω_L varies from 0 to 1.2 eV and V varies from 0.02 to 0.1 eV, initially ignoring the effect of the system-bath interaction, which is incorporated later.

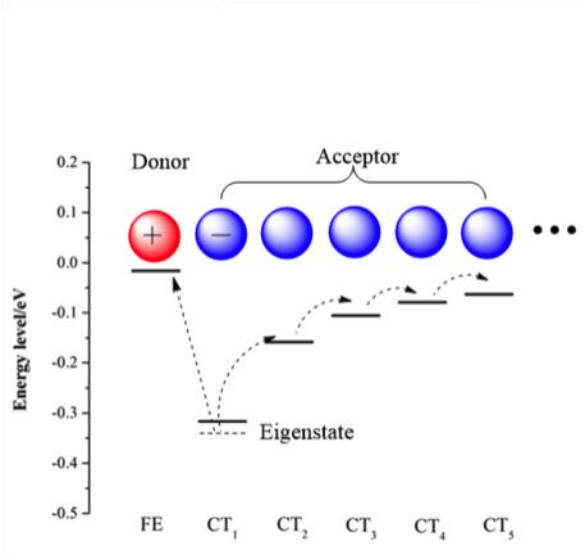

Figure 1. Energy level diagram for an idealized system containing one donor and many acceptor molecules. The Frenkel excitonic state (FE) represents an excitation localized on the donor and the CT_1, CT_2, … states represent CT excitation with increasing separation between hole and electron. The states are localized (diabatic) to build the model Hamiltonian. It is assumed that the lowest eigenstate of this system is the initial state for the excitation by the IR push pulse.

The energy levels involved in our quantum dynamics model are shown in Figure 1. The dynamics of CT states can be traced by the time evolution of the populations of all states, i.e., $P_i(t) = \left|\langle i|\psi(t)\rangle\right|^2$, in which the time-evolution of the wavefunction can be obtained by $\left|\psi(t)\right\rangle = e^{-i\hat{H}t/\hbar}\left|\psi(0)\right\rangle$. Here Chebyshev polynomial expansion is used as a propagation method for the time evolution operator.[45-47]

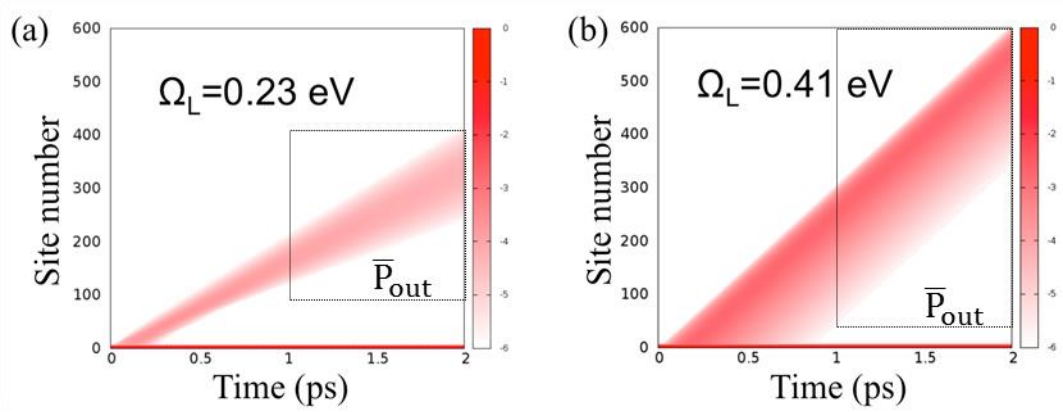

Figure 2. Color-mapped population ($\log P_i$) for different pulse frequencies Ω_L= 0.23 eV (a) and 0.41 eV (b) (these two frequencies are chosen only to illustrate slow/fast charge separation) with V = 0.1 eV, where the vertical axis denotes a site index (the FE state is indexed as site 0).

The charge separation initiated by the pulse field was studied by considering the population on each site as a function of time for different pulse frequencies. Figure 2 illustrates that, following the pulse, the charge density divides into two parts, one propagating outwards from the interface and the other localized either at the bound CT states or on the FE state. The near-linear relationship of the charge position with time indicates that the charge escapes with a near-constant velocity following the pulse. The results with different pulse frequencies shown in Figure 2 suggest that the pulse frequency has a remarkable influence on the charge separation. The lighter and narrower red band for Ω_L = 0.23 eV than the one for Ω_L = 0.41 eV illustrates smaller separated charge and more localized charge for the former than the latter. Besides, the slope of the red band in Figure 2(a) displays smaller than the one in Figure 2(b), which also indicates the slower charge separation velocity of the former than the latter. (Note that we obtain charge dynamics for a full range of pulse frequency and present them in Figures 3 and 4.)

Figure 2 suggests some useful measures that can be used to probe the importance of the various parameters, e.g., what fraction of charge propagates outwards, how far charge can separate, and how fast the outgoing charge will be travelling. Therefore, we first define the outgoing charge as the sum of population on the sites from 4 to N (here the outgoing charge is averaged over the certain time window, i.e., $\bar{P}_{\text{out}} = \frac{1}{\Delta t}\int_{t_0}^{t_0+\Delta t} dt\left(\sum_{i=4}^{N} P_i(t)\right)$). (Note that the total population, i.e., the sum of the population of the FE state, all CT states, and the CT_1* state, is one.) It provides the information on what fraction of charge is leaving the interface on average in time, where charge is considered as "leaving the interface" in this work if it is populated on the acceptor sites with i>3. Second, the expectation value of the position of outgoing charge is defined in the unit of acceptor distance L as follows,

$$\langle x \rangle_{\text{out}} = \frac{\sum_{i=4}^{N} iP_i}{\sum_{i=4}^{N} P_i} \qquad (4)$$

It provides an estimation on how far the outgoing charge can escape from the bound CT states. The escape velocity of outgoing charge can also be used to monitor charge propagation, which is defined as $d\langle x \rangle_{\text{out}} / dt$, obtained by the linear fit of $\langle x \rangle_{\text{out}}$.

Figure 3 describes the averaged population of outgoing charge and the escape velocity with varying pulse frequency Ω_L and different electronic coupling V. It clearly shows that both the population and the escape velocity of outgoing charge are strongly dependent on these parameters. Considering the pulse frequency first, both the population and the escape velocity of outgoing charge have two distinct peaks for every electronic coupling, i.e., one appears at lower Ω_L region (around 0.15 eV for the population and around 0.25 eV for the velocity) and the other

appears at higher Ω_L region (0.3~0.45 eV). For the population shown in Figure 3(a), the smaller peak at around 0.15 eV is related to the transition from the lowest eigenstate to CT_2 state, while the larger peak is related to the transition from the lowest eigenstate to FE state, as we demonstrate below. Besides, the population exhibits sharper peaks than the velocity, suggesting that the amount of charge escaping the interface by the push pulse is more sensitive to the pulse frequency. We note that there is almost no outgoing charge above the pulse frequency ~0.6 eV (not shown in the figure) and therefore the CT_1* state, which lies above 1 eV from the CT_1 state in our simulation, does not play any role in the charge separation induced by the IR pulse.

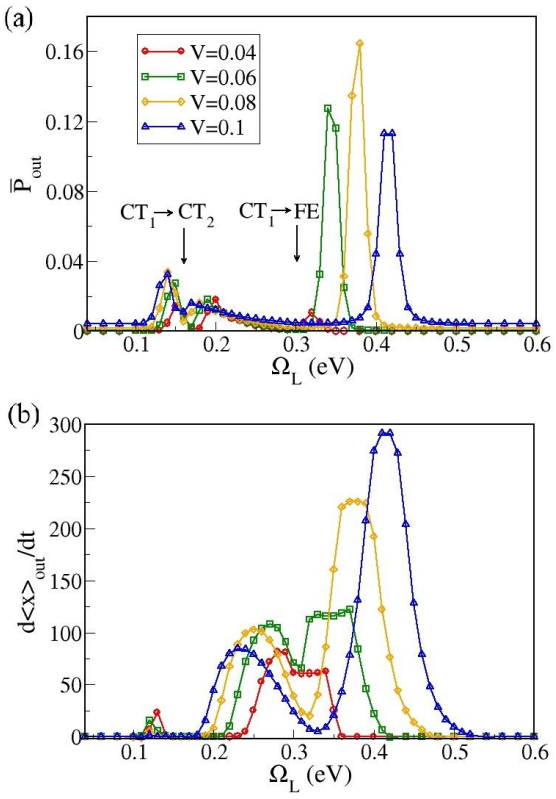

Figure 3. The time-averaged outgoing charge $\bar{P}_{out}$ (a) and the escape velocity of outgoing charge (b) as a function of pulse frequency Ω_L for different electronic coupling values (the corresponding position of the transition energies of $CT_1 \rightarrow CT_2$ and $CT_1 \rightarrow FE$ are marked in Figure (a)). The time-average was over the interval 1-2 ps.

Figure 3 also illustrates the important influence of the electronic coupling V on the charge separation efficiency and the position of the peaks both for the population and the escape velocity. The increase of the electronic coupling up to 0.08 eV leads to the increase of the outgoing charge, while further increase (V=0.1 eV) does not lead to more charge separation. On the other hand, charge separation occurs faster with the increase of the coupling. In contrast to the slight shift to the left of the smaller peak with the increase of the electronic coupling, the larger peak in the high Ω_L region shows a prominent shift to the right. It is ascribed to the enlarged energy difference between the lowest eigenstate and FE state with the increase of the electronic coupling. Accordingly, the range of pulse frequency with efficient charge separation depends on the electronic coupling. Therefore, the electronic bandwidth of the acceptor material also strongly affects the charge separation. It should also be noted that the outgoing population for the larger peak at high Ω_L region with respect to the outgoing population for the smaller peak at low Ω_L region increases with increasing the coupling up to V=0.08 eV. For a realistic system, however, the absolute magnitude also depends on other parameters, e.g. the transition dipole moments. Our work establishes that the two charge-separation mechanisms indicated by the two distinct peaks are expected to be of similar importance.

We next demonstrate the existence of two separate mechanisms of IR-induced charge dissociation. To this end, we obtain the population of the outgoing charge for V=0.06 eV (i) with the transition dipole moment μ between the CT_1 and FE state set to zero and (ii) with the μ between the CT_1 and CT_2 state set to zero (see Figure 4). (The intermediate coupling V=0.06 eV is chosen for the best demonstration of two different mechanisms.) Compared with the two separate peaks at each low and high Ω_L region with non-zero transition dipole moment, we find

that the peak in low Ω_L region (0.1 ~ 0.2 eV) disappears when the μ between the CT_1 and CT_2 state is set to zero and the peak in high Ω_L region (0.3 ~ 0.4 eV) disappears when the μ between the CT_1 and FE state is set to zero. This result clearly demonstrates the promotion effect of the CT_2 and FE state on the charge separation in low and high Ω_L region, respectively. Therefore, the pulse dissociates the CT states following two different mechanisms. One, fairly expected, is the excitation to higher CT states leading to charge separation in low Ω_L region. The other is the excitation of the neutral Frenkel state, followed by the dissociation of this state into free charges in high Ω_L region. Considering that the experimental pulse of ref. 39 (~ 0.5 eV) is close to resonance to the $CT_1 \rightarrow$FE transition, our model suggests that the latter mechanism is more likely to occur in that experiment.

We point out that there are only two important transition dipole moments, the μ between the CT_1 and CT_2 state and the μ between the CT_1 and FE state, and the results only slightly change when the μ between all other adjacent CT states is set to zero (see the dashed line in Figure 4). In this work the $\mu_{CT1,CT2}$ and the $\mu_{CT1,FE}$ were set to the same value based on our quantum chemistry calculation. In realistic situation, however, they will be different possibly in different regions of the same material and therefore two mechanisms cannot be compared exactly. However, they are expected to be of a similar magnitude because, in a single-electron picture, they can be seen as a transfer from the LUMO of the orbital in site 1 to the LUMO orbital in site 2 ($CT_1 \rightarrow CT_2$) or to the LUMO orbital on the donor site ($CT_1 \rightarrow$FE), i.e. a transfer between orbitals in adjacent sites.

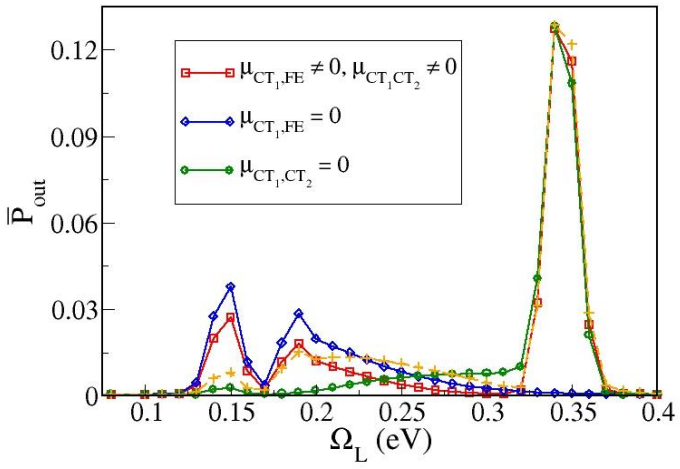

Figure 4. The time-averaged outgoing charge $\bar{P}_{out}$, with the transition dipole moment μ between the CT_1 and FE (or CT_2) state set to zero, is compared to $\bar{P}_{out}$ with the non-zero μ for V=0.06 eV. Dashed line in orange indicates the $\bar{P}_{out}$ with the μ between all CT states set to zero except for $\mu_{CT1,CT2}$.

For a more realistic description of the donor-acceptor interface, we additionally obtained charge dynamics for a two-dimensional (2D) quantum dynamics model as described in SI and found a similar trend of charge dynamics as a function of pulse frequency, i.e., two distinct peaks at higher and lower Ω_L region (see Figure S4 in SI). In addition, we consider the scenario, where the couplings have a Gaussian distribution rather than being a constant, and obtain charge dynamics for different pulse frequencies (see Figure S5 in SI). We still find two different charge-separation mechanisms (direct / rebound) in the case of disordered couplings and that the charge separation via direct mechanism becomes less sensitive to the pulse frequency.

In the model described so far the charge propagates coherently while in reality the interaction with the environment will cause dephasing and relaxation. To estimate the potential effect of the environment, we studied the same model using Redfield theory[48-50] and Drude-Lorentz bath

spectral density $J(\omega) = 2\lambda\omega\omega_c / \left(\omega^2 + \omega_c^2\right)$ for the description of the system-bath interaction, where λ and ω_c^{-1} represent the system-bath coupling strength and the characteristic time scale of the bath correlation function, respectively. For simplicity we switch on the bath when the electric field intensity becomes negligible (at $t = t_0$) and increase the system-bath coupling strength gradually with time, i.e., $\lambda(t) = f(t)\lambda$, where $f(t) = \Theta(t - t_0)\left[1 - \exp\left(-\left(\frac{t - t_0}{\alpha}\right)^2\right)\right]$. (Here the parameter α controls how fast system-bath coupling strength increases and $\Theta(t)$ is the Heaviside step function.) Figure 5 illustrates that the charge propagation slows down and eventually charge starts to relax toward the CT_1 state as the system-bath interaction comes into effect. As well, the oscillatory behavior of charge dynamics gradually disappears. It is seen that, however, the interaction with the thermal environment does not alter the overall trend of charge dynamics, e.g., how it evolves with time for different values of the electronic coupling. Our results therefore suggest that the coupling to the reasonable bath does not change the basic physics of charge dynamics promoted by the IR pulse excitation.

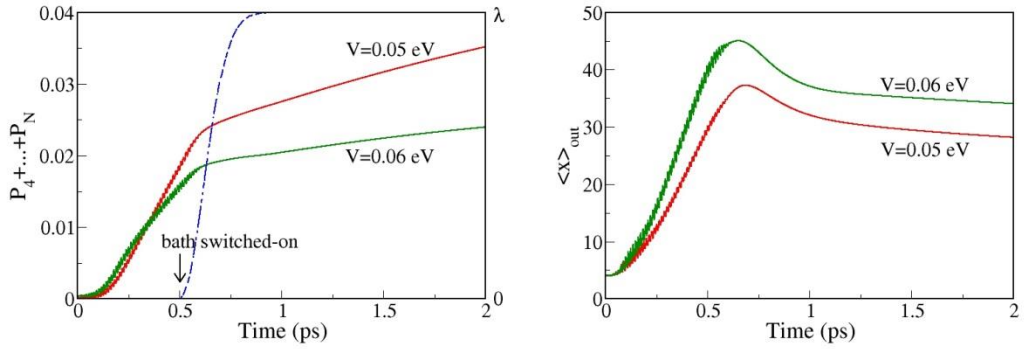

Figure 5. Outgoing charge (left) and expectation value of the position (right) for two different values of V (0.05 and 0.06 eV) and Ω_L = 0.33 eV, where bath parameters are set to λ=0.01 eV,

and ω_c^{-1}=100 fs. Dashed line on the left panel indicates the gradual increase of the system-bath coupling strength with time.

In conclusion, a quantum dynamics model was built to simulate the excitation of CT_1 state by an IR pulse, which has been employed to investigate the properties of bound CT states in experiments. We found that the IR pulse can induce the separation of charges following two different mechanisms: a direct mechanism where the system is directly excited in the CT states manifold and a rebound mechanism where the electron travels in the opposite direction, forming a Frenkel exciton state in the donor, and subsequently the exciton dissociates into free charges from there. The exact path followed depends on the energy of the pulse and the exact energy alignment of the CT and FE states. In our minimalist model, lower energy pulses promote the dissociation via the direct mechanism and higher energy pulses promote the dissociation via the rebound mechanism although in more realistic situation one expects a distribution of FE and CT state energies in proximity of a disordered interface. As a consequence, while IR pulses remain possibly the best probe of the property of CT states, the interpretation of the experimental results can be complicated by the presence of multiple interaction paths.

ACKNOWLEDGEMENTS

Y.G. acknowledges the financial support from the China Scholarship Council (No. 201606625031). A.T. and M.L. acknowledge the support of ERC (Grant No. 615834).

Supporting Information

The Supporting Information contains DFT calculations, 2D quantum dynamics model, the effect of disordered couplings, and the system-bath interaction model in details.

REFERENCES

(1) Bassler, H.; Kohler, A. "Hot or Cold": How Do Charge Transfer States at the Donor-Acceptor Interface of an Organic Solar Cell Dissociate?. *Phys. Chem. Chem. Phys.* **2015**, *17*, 28451-28462.
(2) Brédas, J.-L.; Norton, J. E.; Cornil, J.; Coropceanu, V. Molecular Understanding of Organic Solar Cells: The Challenges. *Acc. Chem. Res.* **2009**, *42*, 1691-1699.
(3) Heeger, A. J. 25th Anniversary Article: Bulk Heterojunction Solar Cells: Understanding the Mechanism of Operation. *Adv. Mater.* **2014**, *26*, 10-28.
(4) Savoie, B. M.; Jackson, N. E.; Chen, L. X.; Marks, T. J.; Ratner, M. A. Mesoscopic Features of Charge Generation in Organic Semiconductors. *Acc. Chem. Res.* **2014**, *47*, 3385-3394.
(5) Zhu, X. Y.; Yang, Q.; Muntwiler, M. Charge-Transfer Excitons at Organic Semiconductor Surfaces and Interfaces. *Acc. Chem. Res.* **2009**, *42*, 1779-1787.
(6) Bakulin, A. A.; Dimitrov, S. D.; Rao, A.; Chow, P. C. Y.; Nielsen, C. B.; Schroeder, B. C.; McCulloch, I.; Bakker, H. J.; Durrant, J. R.; Friend, R. H. Charge-Transfer State Dynamics Following Hole and Electron Transfer in Organic Photovoltaic Devices. *J. Phys. Chem. Lett.* **2013**, *4*, 209-215.
(7) Clarke, T. M.; Durrant, J. R. Charge Photogeneration in Organic Solar Cells. *Chem. Rev.* **2010**, *110*, 6736-6767.
(8) Dimitrov, S. D.; Bakulin, A. A.; Nielsen, C. B.; Schroeder, B. C.; Du, J.; Bronstein, H.; McCulloch, I.; Friend, R. H.; Durrant, J. R. On the Energetic Dependence of Charge Separation in Low-Band-Gap Polymer/Fullerene Blends. *J. Am. Chem. Soc.* **2012**, *134*, 18189-18192.
(9) Tamura, H.; Burghardt, I. Ultrafast Charge Separation in Organic Photovoltaics Enhanced by Charge Delocalization and Vibronically Hot Exciton Dissociation. *J. Am. Chem. Soc.* **2013**, *135*, 16364-16367.
(10) Ryno, S. M.; Fu, Y.-T.; Risko, C.; Brédas, J.-L. Polarization Energies at Organic–Organic Interfaces: Impact on the Charge Separation Barrier at Donor–Acceptor Interfaces in Organic Solar Cells. *ACS Appl. Mater. Inter.* **2016**, *8*, 15524-15534.
(11) Schwarz, C.; Tscheuschner, S.; Frisch, J.; Winkler, S.; Koch, N.; Bässler, H.; Köhler, A. Role of the Effective Mass and Interfacial Dipoles on Exciton Dissociation in Organic Donor-Acceptor Solar Cells. *Phys. Rev. B* **2013**, *87*, 155205.
(12) Tscheuschner, S.; Bässler, H.; Huber, K.; Köhler, A. A Combined Theoretical and Experimental Study of Dissociation of Charge Transfer States at the Donor–Acceptor Interface of Organic Solar Cells. *J. Phys. Chem. B* **2015**, *119*, 10359-10371.
(13) Verlaak, S.; Beljonne, D.; Cheyns, D.; Rolin, C.; Linares, M.; Castet, F.; Cornil, J.; Heremans, P. Electronic Structure and Geminate Pair Energetics at Organic–Organic Interfaces: The Case of Pentacene/C_{60} Heterojunctions. *Adv. Funct. Mater.* **2009**, *19*, 3809-3814.
(14) Gregg, B. A. Entropy of Charge Separation in Organic Photovoltaic Cells: The Benefit of Higher Dimensionality. *J. Phys. Chem. Lett.* **2011**, *2*, 3013-3015.

(15) Hood, S. N.; Kassal, I. Entropy and Disorder Enable Charge Separation in Organic Solar Cells. *J. Phys. Chem. Lett.* **2016**, *7*, 4495-4500.
(16) Ono, S.; Ohno, K. Combined Impact of Entropy and Carrier Delocalization on Charge Transfer Exciton Dissociation at the Donor-Acceptor Interface. *Phys. Rev. B* **2016**, *94*, 075305.
(17) Bittner, E. R.; Silva, C. Noise-Induced Quantum Coherence Drives Photo-Carrier Generation Dynamics at Polymeric Semiconductor Heterojunctions. *Nat. Commun.* **2014**, *5*, 3119.
(18) Falke, S. M.; Rozzi, C. A.; Brida, D.; Maiuri, M.; Amato, M.; Sommer, E.; De Sio, A.; Rubio, A.; Cerullo, G.; Molinari, E. et al. Coherent Ultrafast Charge Transfer in an Organic Photovoltaic Blend. *Science* **2014**, *344*, 1001-1005.
(19) Kocherzhenko, A. A.; Lee, D.; Forsuelo, M. A.; Whaley, K. B. Coherent and Incoherent Contributions to Charge Separation in Multichromophore Systems. *J. Phys. Chem. C* **2015**, *119*, 7590-7603.
(20) Song, Y.; Clafton, S. N.; Pensack, R. D.; Kee, T. W.; Scholes, G. D. Vibrational Coherence Probes the Mechanism of Ultrafast Electron Transfer in Polymer–Fullerene Blends. *Nat. Commun.* **2014**, *5*, 4933.
(21) Wang, T.; Kafle, T. R.; Kattel, B.; Chan, W.-L. A Multidimensional View of Charge Transfer Excitons at Organic Donor–Acceptor Interfaces. *J. Am. Chem. Soc.* **2017**, *139*, 4098-4106.
(22) Athanasopoulos, S.; Tscheuschner, S.; Bässler, H.; Köhler, A. Efficient Charge Separation of Cold Charge-Transfer States in Organic Solar Cells Through Incoherent Hopping. *J. Phys. Chem. Lett.* **2017**, *8*, 2093-2098.
(23) Few, S.; Frost, J. M.; Nelson, J. Models of Charge Pair Generation in Organic Solar Cells. *Phys. Chem. Chem. Phys.* **2015**, *17*, 2311-2325.
(24) Yao, Y.; Xie, X.; Ma, H. Ultrafast Long-Range Charge Separation in Organic Photovoltaics: Promotion by Off-Diagonal Vibronic Couplings and Entropy Increase. *J. Phys. Chem. Lett.* **2016**, *7*, 4830-4835.
(25) Lee, J.; Vandewal, K.; Yost, S. R.; Bahlke, M. E.; Goris, L.; Baldo, M. A.; Manca, J. V.; Voorhis, T. V. Charge Transfer State Versus Hot Exciton Dissociation in Polymer−Fullerene Blended Solar Cells. *J. Am. Chem. Soc.* **2010**, *132*, 11878-11880.
(26) Vandewal, K.; Albrecht, S.; Hoke, E. T.; Graham, K. R.; Widmer, J.; Douglas, J. D.; Schubert, M.; Mateker, W. R.; Bloking, J. T.; Burkhard, G. F. et al. Efficient Charge Generation by Relaxed Charge-Transfer States at Organic Interfaces. *Nat. Mater.* **2014**, *13*, 63-68.
(27) Arndt, A. P.; Gerhard, M.; Koch, M.; Lemmer, U.; Howard, I. A. Identifying Charge-Transfer States in Polymer:Fullerene Heterojunctions by Their Emission Polarization Anisotropy. *J. Phys. Chem. C* **2017**, *121*, 6357-6364.
(28) Bernardo, B.; Cheyns, D.; Verreet, B.; Schaller, R. D.; Rand, B. P.; Giebink, N. C. Delocalization and Dielectric Screening of Charge Transfer States in Organic Photovoltaic Cells. *Nat. Commun.* **2014**, *5*, 3245.
(29) Chen, X.-K.; Ravva, M. K.; Li, H.; Ryno, S. M.; Brédas, J.-L. Effect of Molecular Packing and Charge Delocalization on the Nonradiative Recombination of Charge-Transfer States in Organic Solar Cells. *Adv. Energy Mater.* **2016**, *6*, 1601325.
(30) Deotare, P. B.; Chang, W.; Hontz, E.; Congreve, D. N.; Shi, L.; Reusswig, P. D.; Modtland, B.; Bahlke, M. E.; Lee, C. K.; Willard, A. P. et al. Nanoscale Transport of Charge-Transfer States in Organic Donor-Acceptor Blends. *Nat. Mater.* **2015**, *14*, 1130-1134.

(31) Fazzi, D.; Barbatti, M.; Thiel, W. Unveiling the Role of Hot Charge-Transfer States in Molecular Aggregates via Nonadiabatic Dynamics. *J. Am. Chem. Soc.* **2016**, *138*, 4502-4511.
(32) Gélinas, S.; Paré-Labrosse, O.; Brosseau, C.-N.; Albert-Seifried, S.; McNeill, C. R.; Kirov, K. R.; Howard, I. A.; Leonelli, R.; Friend, R. H.; Silva, C. The Binding Energy of Charge-Transfer Excitons Localized at Polymeric Semiconductor Heterojunctions. *J. Phys. Chem. C* **2011**, *115*, 7114-7119.
(33) Graham, K. R.; Ndjawa, G. O. N.; Conron, S. M.; Munir, R.; Vandewal, K.; Chen, J. J.; Sweetnam, S.; Thompson, M. E.; Salleo, A.; McGehee, M. D. et al. The Roles of Structural Order and Intermolecular Interactions in Determining Ionization Energies and Charge-Transfer State Energies in Organic Semiconductors. *Adv. Energy Mater.* **2016**, *6*, 1601211.
(34) Hedley, G. J.; Ruseckas, A.; Samuel, I. D. W. Light Harvesting for Organic Photovoltaics. *Chem. Rev.* **2017**, *117*, 796-837.
(35) Liu, X.; Ding, K.; Panda, A.; Forrest, S. R. Charge Transfer States in Dilute Donor–Acceptor Blend Organic Heterojunctions. *ACS Nano.* **2016**, *10*, 7619-7626.
(36) Liu, Y.; Zojer, K.; Lassen, B.; Kjelstrup-Hansen, J.; Rubahn, H.-G.; Madsen, M. Role of the Charge-Transfer State in Reduced Langevin Recombination in Organic Solar Cells: A Theoretical Study. *J. Phys. Chem. C* **2015**, *119*, 26588-26597.
(37) Nan, G.; Zhang, X.; Lu, G. The Lowest-Energy Charge-Transfer State and its Role in Charge Separation in Organic Photovoltaics. *Phys. Chem. Chem. Phys.* **2016**, *18*, 17546-17556.
(38) Zhu, X.; Monahan, N. R.; Gong, Z.; Zhu, H.; Williams, K. W.; Nelson, C. A. Charge Transfer Excitons at van der Waals Interfaces. *J. Am. Chem. Soc.* **2015**, *137*, 8313-8320.
(39) Bakulin, A. A.; Rao, A.; Pavelyev, V. G.; van Loosdrecht, P. H. M.; Pshenichnikov, M. S.; Niedzialek, D.; Cornil, J.; Beljonne, D.; Friend, R. H. The Role of Driving Energy and Delocalized States for Charge Separation in Organic Semiconductors. *Science* **2012**, *335*, 1340-1344.
(40) Jakowetz, A. C.; Böhm, M. L.; Zhang, J.; Sadhanala, A.; Huettner, S.; Bakulin, A. A.; Rao, A.; Friend, R. H. What Controls the Rate of Ultrafast Charge Transfer and Charge Separation Efficiency in Organic Photovoltaic Blends. *J. Am. Chem. Soc.* **2016**, *138*, 11672-11679.
(41) D'Avino, G.; Muccioli, L.; Olivier, Y.; Beljonne, D. Charge Separation and Recombination at Polymer–Fullerene Heterojunctions: Delocalization and Hybridization Effects. *J. Phys. Chem. Lett.* **2016**, *7*, 536-540.
(42) Lee, M. H.; Aragó, J.; Troisi, A. Charge Dynamics in Organic Photovoltaic Materials: Interplay between Quantum Diffusion and Quantum Relaxation. *J. Phys. Chem. C* **2015**, *119*, 14989-14998.
(43) Smith, S. L.; Chin, A. W. Ultrafast Charge Separation and Nongeminate Electron-Hole Recombination in Organic Photovoltaics. *Phys. Chem. Chem. Phys.* **2014**, *16*, 20305-20309.
(44) Troisi, A. How Quasi-Free Holes and Electrons are Generated in Organic Photovoltaic Interfaces. *Faraday Discuss.* **2013**, *163*, 377-392.
(45) Kosloff, R. Propagation Methods for Quantum Molecular Dynamics. *Annu. Rev. Phys. Chem.* **1994**, *45*, 145-178.
(46) Leforestier, C.; Bisseling, R. H.; Cerjan, C.; Feit, M. D.; Friesner, R.; Guldberg, A.; Hammerich, A.; Jolicard, G.; Karrlein, W.; Meyer, H. D. et al. A Comparison of Different Propagation Schemes for the Time Dependent Schrödinger Equation. *J. Comput. Phys.* **1991**, *94*, 59-80.

(47) Tal-Ezer, H.; Kosloff, R. An Accurate and Efficient Scheme for Propagating the Time Dependent Schrödinger Equation. *J. Chem. Phys.* **1984**, *81*, 3967-3971.
(48) May, V.; Kühn, O. *Charge and Energy Transfer Dynamics in Molecular Systems*; Willey-VCH: Berlin; 2011.
(49) Nitzan, A. *Chemical Dynamics in Condensed Phases*; Oxford University Press: New York; 2006.
(50) Redfield, A. G. On the Theory of Relaxation Processes. *IBM J. Res. Dev.* **1957**, *1*, 19-31.